Inelastic interactions of protons and electrons with biologically relevant molecules

B. Coupier, B. Farizon, M. Farizon, M.J. Gaillard, F. Gobet, N.V. de Castro Faria, G. Jalbert, S. Ouaskit, M. Carre, B. Gstir, et al.

EPJ D proofs
(will be inserted by the editor)

Inelastic interactions of protons and electrons with biologically relevant molecules

B. Coupier[1], B. Farizon[1], M. Farizon[1,a], M.J. Gaillard[1], F. Gobet[1], N.V. de Castro Faria[1,b], G. Jalbert[1,b], S. Ouaskit[1,c], M. Carré[2], B. Gstir[3], G. Hanel[3], S. Denifl[3], L. Feketeova[3], P. Scheier[3], and T.D. Märk[3]

[1] Institut de Physique Nucléaire de Lyon, IN2P3-CNRS et Université Claude Bernard, 43 boulevard du 11 novembre 1918, 69622 Villeurbanne Cedex, France
[2] Laboratoire de Spectrométrie Ionique et Moléculaire, CNRS[d] et Université Claude Bernard, 43 boulevard du 11 novembre 1918, 69622 Villeurbanne Cedex, France
[3] Institut für Ionenphysik, Leopold Franzens Universität, Technikerstr. 25, 6020 Innsbruck, Austria

Received 25 February 2002
Published online ??? –

Abstract. Ionization and fragmentation of water and uracil molecules was studied both by electron and proton impact. A special coincidence technique allows on an event by event basis the investigation of product ions formed upon the collision of protons with neutral molecules including the identification of the charge state of the projectile. This enables the characterization of the ionization processes occurring, *i.e.* direct ionization, single electron capture or double electron capture for 0, 1 or 2 electrons that are transferred from the target to the projectile, respectively. For uracil the fragmentation patterns obtained by electron and proton impact ionization reveal close similarities and indicate a comparable amount of excitation for the two different ionization mechanisms at high enough projectile energies.

PACS. 87.50.Gi Ionizing radiations (ultraviolet, X-rays, γ-rays, ions, electrons, positrons, neutrons, and mesons, etc.) – 87.14.Gg DNA, RNA – 34.50.Gb Electronic excitation and ionization of molecules; intermediate molecular states (including lifetimes, state mixing, etc.)

1 Introduction

It is generally considered that the types of primary damage induced in DNA by ionizing radiation that lead to the most significant biological effects are double-strand breaks (DSB) [1] and clustered lesions. These types of lesion have the greatest relevance to cellular effects underlying both human cancer risk from radiation exposure and the cell killing action of radiation used in radiotherapy. Clustering of strand breaks and base damages formed where radiation tracks cross the DNA molecule are believed to have the greatest significance and this view is supported by experimental evidence coupled with information from modeling studies. Although the development of mechanistic models of radiation damage in DNA has reached a high level of sophistication, further refinements are needed to understand fully the underlying mechanisms in particular on a molecular level. The present study – the first in a series from the two laboratories in Lyon and Innsbruck involved – are designed to provide in a comprehensive manner missing information about the molecular pathways that lead from initial deposition of radiative energy to the formation of lesions in DNA.

The genotoxic effects of ionizing radiation (α, β, γ, ions) in living cells are produced not only by the direct impact of the primary high-energy projectiles but also by secondary species generated by the primary ionizing radiation, *e.g.*, free electrons with low energies, typically below about 20 eV. Therefore, it is recognized that radiation action in bio-molecules cannot only be described by the interaction of the primary encounter between radiation and molecule involved, but that the simultaneous and consecutive action of the primary, secondary and tertiary species (including also radicals such as OH formed by the destruction of the water molecules surrounding the DNA) have to be included in any quantitative consideration about radiation damage.

Therefore, the presently initiated studies will concentrate on the effects of primary radiation (high energy protons) as well as reactions of secondary low energy electrons. These studies will be performed using several selected prototypical biomolecules as targets. In the present report we will present in an illustrative manner first re-

[a] e-mail: mfarizon@ipnl.in2p3.fr
[b] *Permanent address*: Instituto de Fisica, Universidade Federal do Rio de Janeiro, Rio de Janeiro 21945-970 RJ Brazil.
[c] *Permanent address*: Département de Physique, Université Hassan II, Faculté des sciences Ben M'sik, Casablanca, Morocco.
[d] UMR 5579

sults obtained for a simple molecule, *e.g.* H_2O, as well as on more complex bio-molecule such as uracil. The very recent development, refinement and application of new experimental techniques in our laboratories (*e.g.*, novel types of beam sources, multi-coincidence detection techniques, high resolution beam and mass spectrometry techniques) makes this the ideal time for carrying out a coordinated series of experiments planned to attack the many open questions in this field.

The ionization of water molecules represents not only a fundamental example in collision physics [2], but it is also of great interest in several areas of applied physics spanning the range from radiation damage in biological tissues [3], over the chemistry of the upper planetary atmospheres [4] to the ionization balance in the plasma of tokamak fusion devices [5]. In spite of the broad range of interest, cross-section measurements concerning water are scarce and a number of details have not been investigated up to now. Most studies so far have been restricted to electron impact ionization, including a small number of partial and total ionization cross-section studies (see Refs. [6,7] and references therein). Moreover, cross-sections for the ionization of water by ion impact are extremely rare. In 1968, Toburen *et al.* [8] reported the first total electron capture cross-sections for protons in H_2O in the energy range 100–2 500 keV. In 1977, Toburen and Wilson [9] have measured doubly differential ionization cross-sections for 300–1 500 keV proton in H_2O and, in 1986, this study was extended downward to an energy range 15–150 keV by Bolorizadeh and Rudd [10]. Toburen *et al.* [11] have also reported similar measurements for He^+ and He^{++} ions for 300–2 000 keV. Their experiment was followed in 1985 by a study of Rudd *et al.* [12] providing absolute total cross-sections for proton ionization of water vapor from 7–4 000 keV (see also a theoretical study on single differential cross-sections of water vapor [13]). More recently, Lutz and co-workers [14] have reported for the first time the investigation of multiple ionization and fragmentation of water after 100–400 keV proton impact, using a position and time-sensitive multi-particle detector. Using a correlation technique they were able to detect positive ions from the molecular break-up process. Besides total and partial single ionization, as well as multiple ionization and fragmentation cross-sections, their data contain information on the kinetic energy release and the angular correlation for each individual impact event. However, their specialized set-up was only sensitive to positive ions produced from water. In particular they could not detect neutralized projectiles and thus obtain the important information on individual electron-capture cross-sections. Despite numerous studies on total capture cross-sections for incident protons in various gases [15–17], today there still do not exist any results on partial electron capture cross-sections.

Here we report on the application of an experimental set-up developed in Lyon which allows us, on an event by event basis, to analyze in great detail proton impact ionization of water vapor and to measure partial and total single ionization cross-sections as a function of the charge state of the projectile after the ionization event. We are able to obtain mass analyzed product ion signals (*e.g.*, H_2O^+, OH^+, O^+, O^{++}, H^+, and also negative ions) in coincidence with the charge-analyzed projectile, *i.e.*, after the ionizing collision the proton can either be an H^+ or after single electron capture during the ionization event a neutral H or H^- after double electron capture. The present study became possible after the addition of a time of flight mass spectrometer [18] operated in coincidence with our existing high-energy ion beam multi-coincidence apparatus [19,20]. In contrast to the earlier correlation experiment by Lutz and coworkers [14] we are now able to analyze the fate of the projectile in coincidence with the fate of the target molecule. For the first time we are thus able to provide ionization and dissociation cross-sections that are "differential" in terms of the projectile state. Due to the outstanding role of H_2O in radiation damage of biological tissue we have selected this molecule for the present, exploratory study. Here we report only on results involving positive product ion formation, direct ionization and single electron capture events. Moreover, recently, we have extended these studies to uracil and we have obtained first proton induced mass spectra for this molecule.

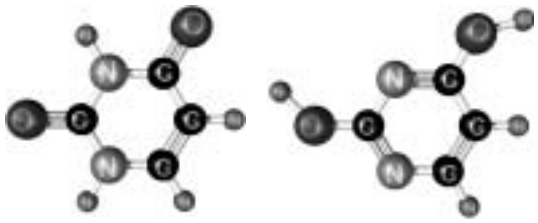

Fig. 1. The possible two tautomeric forms of uracil, the left one being the one obtained under optimized geometry situation from a DFT calculation by Schermann *et al.* [21] and the right one being the one shown in the NIST webbook.

Uracil is one of the four bases in RNA [21,22]. The others are adenine, guanine, and cytosine. Uracil replaces thymine, which is the fourth base in DNA. Like thymine, uracil always pairs with adenine. Figure 1 shows schematically the structure of this molecule (for details of the optimized geometries of the uracil molecule and its anion see Refs. [23,24]). Uracil was for the first time isolated from herring sperm and also produced in a laboratory at the beginning of the 20th century. When combined with the sugar ribose in a glycosidic linkage, uracil forms a derivative called uridine (a nucleoside), which in turn can be phosphorylated with one to three phosphoric acid groups, yielding respectively the three nucleotides UMP (uridine monophosphate), UDP (uridine diphosphate), and UTP (uridine triphosphate). The analogous nucleosides and nucleotides formed from uridine and deoxyribose occur only very rarely in living systems; such is not the case with the other pyrimidines. The nucleotide derivatives of uracil perform important functions in cellular metabolism, particularly in carbohydrate metabolism; UTP acts as a coenzyme in the biosynthesis of sucrose in plants, lactose and glycogen in mammals, and chitin in insects. It can also readily donate one of its phosphate groups to adenosine diphosphate (ADP) to form adenosine triphosphate

(ATP), an extremely important intermediate in the transfer of chemical energy in living cells. Since the uracil nucleotides contain only ribose and not deoxyribose, UTP is the source of uridine only in ribonucleic acid (RNA); there is no uridine in deoxyribonucleic acid (DNA). Its involvement in the biosynthesis of RNA demonstrates that uracil is important in the translation of genetic information. A few laboratory derivatives of uracil have been designed as experimental antimetabolites for use in cancer chemotherapy [25].

Theoretical predictions and measurements of ionization energies, electron affinities and cross-sections for small molecules of biological interest such as DNA and RNA bases represent a difficult task due to a number of reasons. For instance, one problem for the determination of electron affinities of DNA and RNA bases comes from the large polarity of these molecules which allows the existence of two very different types of anions, *i.e.*, involving valence or dipole bound electrons. This problem has been resolved recently in a pioneering study by Schermann and co-workers [23,26] using Rydberg electron attachment to gas phase isolated uracil molecules and mixed uracil-argon clusters. By means of reproducible uracil beam conditions it was possible to control the electron attachment process which is strongly depending on solvation. In extending these measurements we are here investigating the production of positive ions of uracil produced by electron or proton impact.

In addition to the studies on proton ionization of uracil accomplished in Lyon employing the coincidence apparatus mentioned above we have also carried out in Innsbruck mass spectrometric studies of uracil using a high resolution electron spectrometer yielding detailed information on the mass spectrum as well as some preliminary information on appearance energies. The heart of this instrument is a hemispherical electron monochromator that enables both the production of positively and negatively charged ions with an electron energy resolution better than 100 meV. In the following we will first present the two experimental set-ups used in Lyon and in Innsbruck. In Section 3 we will present results pertaining to proton ionization of water and in Section 4 we will discuss first preliminary results obtained for the ionization of uracil with protons and electrons, respectively.

2 Experimental

2.1 The Lyon proton beam apparatus

The experiments in Lyon were carried out with a newly developed crossed beams instrument that is shown schematically in Figure 2. Pure molecular hydrogen is ionized in a standard RF-discharge source (80 MHz). Typical parameters for the ion source are 30 W RF-power and a pressure of about 1 Pa. The whole ion source is mounted on a high voltage terminal of an accelerator that allows kinetic energies of singly charged ions up to 150 keV with a resolution $\Delta E/E$ of 0.01 [27]. Accelerated protons are separated from other ions like H_2^+, H_3^+ and ions originating

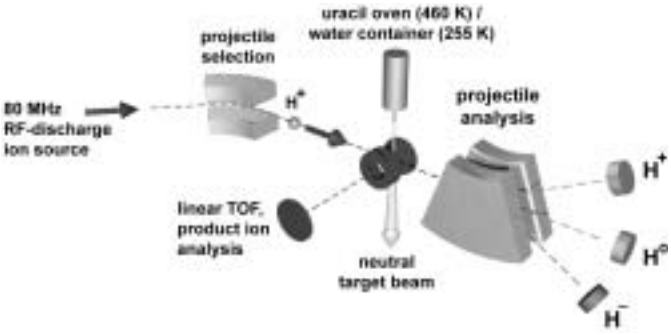

Fig. 2. Schematic view of the Lyon crossed beam coincidence apparatus. The product ions analyzed by the linear TOF are measured in coincidence with the charge state analyzed projectile. Moreover, using a (charge exchange) gas cell in front of the interaction region and a deflector plate it is possible to perform these experiments also with fast neutral projectiles.

from impurities in the source by means of a magnetic sector field. After tight collimation of the primary ion beam (two circular apertures of 0.5 mm radius, about 1 meter apart) the proton beam is crossed at right angles with an effusive beam of water or uracil molecules. Distilled water that has been degassed prior to the experiment in freezing, pumping and thawing cycles is kept during the measurements at a temperature of 255 K. The vapor above the ice is introduced through a capillary that is kept at room temperature. Uracil powder is evaporated from a temperature-controlled oven at temperatures between 450 K and 465 K. The oven [28] is mounted on a micrometric goniometer which allows (x, y) translation by steps of 50 μm. The opening of the oven has a diameter of 1 mm and is located 2 mm under the proton beam. The distance between the exit of the oven and the centered proton beam is as short as possible in order to increase the density of the neutral target beam. The charge state of the projectile ions after the collision with a target molecule can be determined with a magnetic analyzer and three channeltron type secondary electron multipliers located at the appropriate positions to measure H^+, H^0 and H^-. A home built linear time of flight mass spectrometer (TOF) is used to investigate all product ions formed upon proton impact on water or uracil molecules, respectively. Both positively and negatively charged ions are analyzed. However, for the present investigation only positively charged product ions were investigated. The ions are extracted from the interaction region of the proton and the neutral target beam perpendicular to the direction of both. The extraction and subsequent acceleration field fulfill the conditions defined by Wiley and McLaren [29]. The mass resolution of the TOF is sufficiently high to clearly separate H_2O^+, OH^+ and O^+ (see Fig. 3, upper part). For uracil, however, product ions with a mass per charge ratio larger than 28 cannot be separated from their neighboring ions of a mass per charge ratio that differs less than 1 Thomson (see Fig. 3, lower part). The dashed lines are the resulting curves of multiple Gaussian fits to the experimental data (indicating the presence of several ion peaks, see below) and the

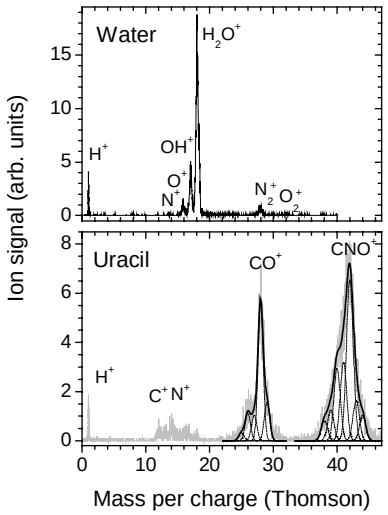

Fig. 3. Product ion mass spectra (see also text) for proton impact ionization of water (upper part) and uracil (lower part) in coincidence with a positively charged projectile (direct ionization). Both mass spectra were obtained by adding up the ion signals measured at all projectile energies, *i.e.* from 20 keV to 150 keV.

dark line is the corresponding superposition of these single peaks.

For the present work it is of great importance that the projectile beam is free of fast hydrogen atoms that were formed by the neutralization of protons due to collisions with surfaces or gas particles. Thus the vacuum has to be better than 10^{-4} Pa all along the beam line and the alignment of the proton beam is carefully checked prior to the experiment. Furthermore, single collision conditions are necessary to guarantee unambiguous identification of the reactions to be studied. This is checked by variation of the density of the water beam in order to exclude reactions between hydrogen atoms (neutralized by electron capture from a target molecule) and further target molecules.

The flight time in the TOF and thus the mass per charge ratio of the "product" ions was determined in the present work by a special technique. Often in similar experiments secondary electrons create a start signal at a detector that is located opposite to the product ion detector. However, in the present study we are also interested in events where ions are produced from water *via* electron capture processes and instead of a free electron emission the charge state of the projectile is changed. On the other hand each proton that crosses the interaction region can be detected in the present experiment independently of the charge state after a collision with a target molecule. The energy transfer during such a collision can be neglected compared to the kinetic energy of the proton beam (20–150 keV). If a "product" ion is formed the channeltron detector of the TOF will produce a pulse. The difference between the time corresponding to this pulse and the time corresponding to the detection of the projectile is used to measure the flight time of the different product ions. The intensity of the proton beam is adjusted in order to avoid the observation of two ionization events during the largest time of flight of the "product" ions.

In contrast to earlier experiments [8–12,14,30,31] the present method provides simultaneously information on the mass per charge ratio of the product ion that is formed and the fate of the projectile ion. This allows us to distinguish between direct ionization and electron capture during the ionization process for each collision event with the additional knowledge of the "product" ions formed. Furthermore, this technique also allows the identification of processes where two or more product ions are formed in one collision event. For instance Coulomb explosion of multiply charged H_2O molecules that has been observed and studied in detail by Werner *et al.* [14] can also be identified with the present setup.

2.2 The Innsbruck electron beam apparatus

The apparatus used for the present experiments, described in detail previously [32–34], consists of an electron monochromator, a sample inlet system, a collision chamber, a mass filter for the product ion analysis, and an ion collection system. This instrument was primarily built in our Innsbruck laboratory for the study of electron-particle interactions under high sensitivity and high-energy resolution. In a temperature controlled oven uracil powder is evaporated between 450 K and 460 K. The opening of the oven has a diameter of 1 mm and is located only a few mm in front of the collision chamber with the electrons. The distance of the oven opening to the electron beam is as short as possible (less than 2 cm) in order to increase the density of the neutral target beam.

The monochromatized electrons (with typical currents in the present study of about 50 nA, see also below) are produced by a standard home-built hemispherical electron monochromator (HEM) whose performance has been improved by careful attention to a number of technical details. The hemispheres, the sample inlet system and all electron-ion-optical elements are made of a single material (stainless steel) to improve uniformity of surface potentials. Frequent bake-outs are invoked to reduce contamination of the surfaces by the sample gas. In the case of uracil however, the temperature of the monochromator and ion optical lenses is too low to prevent condensation of gaseous uracil and thus non conductive ad-layers have to be removed frequently. Residual magnetic fields in the whole instrument are kept below 0.003 gauss with Helmholtz coils compensating the earth's magnetic field. Ferromagnetic materials were avoided in the vicinity of the electron beam. All voltages applied to the electron-ion-optical elements are supplied by a specially constructed power supply with a ripple of $\leq$1 mV.

Ions formed in the collision chamber are extracted on line to the neutral beam direction by a weak electric field. Usually, a rather low ion extraction voltage of about 50 mV (corresponding to an electric field strength of about 0.12 V/cm) was used in order to minimize disturbing field effects. The extracted ions are then focused by a system of electrostatic lenses into the entrance of a quadrupole mass

spectrometer with a nominal mass range of 2 000 amu. The mass-selected ions are detected by a channeltron multiplier operated in single ion counting mode.

One way to check the performance of the instrument is the measurement of the Cl^- production *via* dissociative electron attachment (DEA) to CCl_4 at incident energies, E, close to zero eV [32]. In this case the width of the "zero-energy" DEA peak is determined by the convolution of the finite electron beam distribution and the rapidly decreasing s-wave cross-section function so that the full width at half maximum (FWHM) gives a convenient measure for the energy spread of the electron beam. In the present experiment an improved version of our HEM developed recently gave at best an energy spread of about 30 meV. Nevertheless, for the present measurements an energy resolution of approximately 100 meV has been used in order to achieve electron currents large enough (approximately 50 nA) to obtain large enough ion signals allowing to study ions produced with small cross-sections. The "zero-energy" Cl^-/CCl_4 peak position was also used for calibration of the energy scale at low energies, the O^- onset for DEA to CO at an electron energy of 9.6 eV (for details see [32]).

In addition appearance energies for the production of singly charged cations of various test gases (including rare gases and molecular gases) have been measured and used to support the electron energy scale calibration discussed above involving electron attachment. The appearance energies of the product cations were derived using a novel data handling procedure described in details in recent publications [33,34]. In short, the measured ionization cross-section were fitted with a non-linear weighted least squares fit of the raw data using the Marquart-Levenberg algorithm. The fit function $F(E)$ is fitted over an energy range which incorporates the threshold region:

$$f(E) = b + c(E - AE)^p. \quad (1)$$

The fit then involves four parameters; b the background signal, AE the appearance energy, a scaling factor c that is set to zero below AE and to a constant value for $E > AE$. p is an exponential factor, which according to Wannier [35] should be 1.127 in the case of the hydrogen atom (for more details on theoretical predictions for the threshold law see [28]). The data was fitted over an energy range from below the AE (where the only signal is background) to some 3 eV above AE. As a test of the accuracy of the fitting method (and the linearity of the energy scale) the ionization cross-sections of some rare gases and some simple molecules were measured and appearance energies for cations derived. Excellent agreement (within about 10 meV) was found with standard values (NIST data base [36]), using Xe as a standard gas to calibrate the energy scale. From these results we conclude that the present fitting technique gives reliable appearance energies for cations produced by electron impact ionization and that the estimated accuracy of the energy scale is <10 meV and exhibits also a good linearity in the energy range (appr. 0 to 20 eV) covered by these methods.

Recently we have measured in detail the He^+ ionization cross-section function in the electron energy range from approximately 56 to 59 eV. By fitting the two structures corresponding to the presence of the two triply excited $n = 2$ intra-shell He^- resonances $(2s^2 2p)^2P$ and $(2s^2 p^2)^2D$ with the theoretical natural line shape we have deduced their energy positions to lie at 57.03±0.05 eV and 58.13 ± 0.05 eV, respectively [37]. These two resonances can be used in addition to calibrate our energy scale up to about 60 eV.

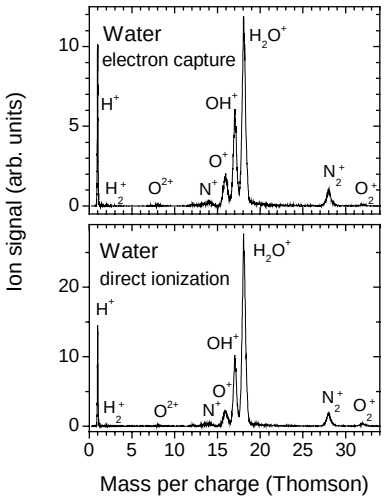

Fig. 4. Product ion mass spectra for proton impact ionization of water. The ion yield shown in the upper part of the figure was measured in coincidence with a neutralized projectile (single electron capture) and the mass spectrum shown in the lower part of this figure was obtained in coincidence with an unchanged charge state of the projectile (direct ionization). In order to increase the statistics both mass spectra represent a summation of the ion yield measured at all different projectile energies. Furthermore, discrimination of fragment ions due to their initial kinetic energy is corrected applying a special calibration method described in the text.

3 Proton impact ionization of water molecules

Figure 4 shows the product ion mass spectra obtained by the collision of protons with water molecules in the energy range of 20 keV to 150 keV. In order to increase the statistics we added up ion signal obtained at different projectile energies. This allows the identification of product ions that are formed with low cross-sections such as the H_2^+ ion. The upper part of Figure 4 represents the product ions that are formed upon an electron transfer from the target molecules to the proton thus transforming it into a fast neutral hydrogen atom. If only one singly charged product ion is generated no free electron will be released. This is the reason why the mass of the product ions is not determined utilizing the released electrons. The lower part of this figure shows the product ions that are formed without changing the charge state of the projectile. Therefore these processes always release at least one electron. Double electron capture [38], *i.e.* the formation of an H^-, was

practically not observed in coincidence with product ions. Figure 4 clearly reveals that for electron capture processes the relative abundance of fragment ions is larger than for direct ionization. For electron capture 49% and for direct ionization only 40% of the total product ion yield is due to fragment ions.

Instead of a multi channel plate detector which is normally used in combination with a TOF mass spectrometer a channeltron type SEM was used in the present study. On the one hand this increases the probability for the detection of a product ion due to the fact that only a certain fraction of the surface of a channel plate is active (the micro channels itself). But on the other hand the time and mass resolution is reduced and furthermore, the detection efficiency for product ions that are formed with initial kinetic energy is lowered too due to the smaller geometric size of the detector. For water the lower mass resolution does not matter at all since all the product ions are clearly separated in the mass spectra. However, in many processes that lead to the formation of a fragment ion kinetic energy is released and distributed to the fragments according to momentum conservation. Therefore, especially for light fragments like H^+ and H_2^+ a significant part of the generated ions will miss the detector [39].

Werner *et al.* [14] published absolute partial cross-sections for the ionization of water by proton impact in the energy range between 100 and 350 keV. However, they only considered collision events where at least one free electron was produced (direct ionization plus electron capture processes that lead to the formation of more than one ion or to a multiply charged product). In order to compare the present data with the cross-sections published by Werner *et al.* one would have to add the events of double ionization and multi ion formation for electron capture to the direct ionization processes. For all singly charged product ions multiple ionization processes due to electron capture contribute however with less than 10% to this corrected fragment ion yield. The target thickness and both, the intensity and shape of the primary ion beam were not constant in the present study for measurements at different projectile energies. The detection of the parent ion H_2O^+ can be considered to be free of discrimination losses due to kinetic energy release upon a fragmentation process. The ratio of the corrected ion yield of a fragment ion and the H_2O^+ ion signal will cancel the effects of unknown target thickness and differing projectile ion beam properties but still contains the information about the discrimination due to the kinetic energy of the fragment ion just after its formation. In Figure 5 these ion yield ratios are plotted as a function of the projectile energy (filled symbols). In addition, the ratio of and cross-section data for fragment ions and H_2O^+ published by Werner *et al.* [14] are shown with open symbols. For heavy fragment ions the two data sets do not differ much but in the case of the formation of a proton the present data (filled triangles) are significantly smaller than the corresponding ratios calculated from the cross-sections of Werner *et al.* [14]. This confirms that the present TOF indeed has a reduced detection efficiency for fragment ions formed with kinetic

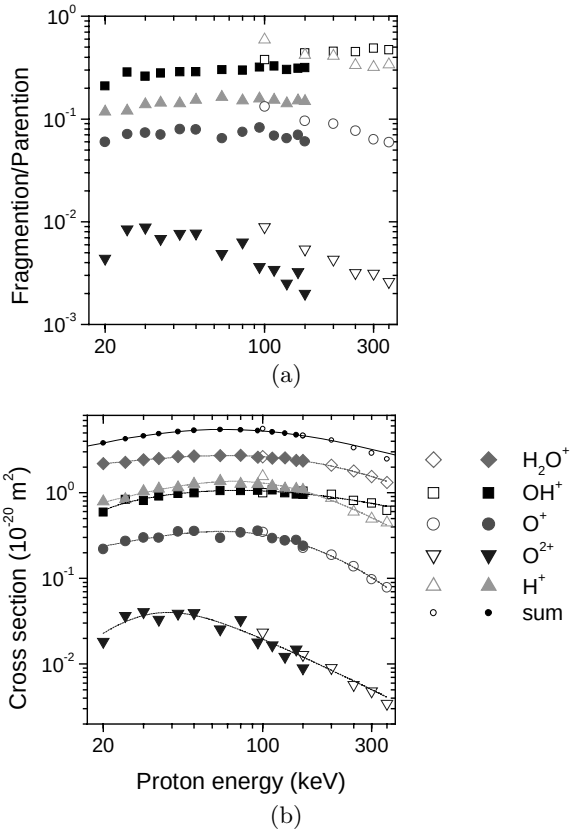

Fig. 5. Upper part (a): ratios of the ion yields of the fragment ions and the parent ion H_2O^+ as a function of the projectile energy. The filled symbols represent the present data and the open symbols are taken from Werner *et al.* [14]. The difference in the signal intensity between two corresponding data sets is due to reduced detection efficiency in the present experiment. The lower part (b) of this figure shows the same data sets after correction of the present data (see text). The dashes lines are fits of equation (2) to the experimental data. Furthermore, the relative cross-section data were normalized with the total cross-section of Rudd *et al.* [12].

energy release. For each fragment ion a discrimination factor was determined that corrects the present data and matches the two curves in the energy regime where they overlap. Based on the assumption that the discrimination due to kinetic energy release is independent of the projectile energy the ion yield of each fragment ion was corrected at all projectile energies with the corresponding factor derived from Figure 5. The Mass spectra in Figure 4 have been corrected with respect to this discrimination of the fragment ions. It should be noted that in our earlier preliminary presentation of part of these data [34] not all of these corrections were taken into account.

From the present data absolute cross-sections could be derived if the target density, the ion current of the projectile beam and the geometric overlap of the proton beam with the water molecule beam is known. The projectile ion current was determined for each measurement and the target density is supposed to be the constant and depends almost exclusively on the temperature of the ice. However,

the overlap factor between the two beams is unknown and might have changed at different projectile energies. Therefore, the present data have to be normalized at each energy to a published cross-section. Rudd *et al.* [12] determined the absolute total cross-section of water for proton energies between 7 and 4 000 keV. Furthermore, they also measured the cross-sections for processes that lead to the production of a negatively charged particle. They called this cross-section σ_- and assumed that it originates exclusively from electrons and neglected the formation of anions. The present experimental setup allows the analysis of anions and indeed the formation of negatively charged ions upon the proton impact to water has not been observed. The total cross-section that leads to the formation of any positively charged product ion is designated σ_+. It is possible to calibrate the present measurements for the total ion production with σ_+ as done previously [40]. Alternatively it is possible to calibrate the relative cross-sections with the ion yield of the product ions that have been formed by the emission of electrons (σ_-). It turns out that the two possibilities lead to the same result except for the very low projectile energies. A calibration with σ_- will lead to smaller errors for the cross-sections of direct ionization which has certain advantages for a comparison between proton and electron impact ionization.

Rudd *et al.* published a formula that allows the calculation of σ_- for a proton energy E_p:

$$\sigma_-(E_\mathrm{p}) = \frac{4\pi a_0^2}{\dfrac{x}{A\ln(1+x)+B} + \dfrac{1}{Cx^D}} \qquad (2)$$

with $x := (E_\mathrm{p}/1\,836)/13.6\,\mathrm{eV}$, a_0 the Bohr radius and four constants ($A = 2.89$, $B = 4.42$, $C = 1.48$ and $D = 0.75$) that were determined by fitting equation (1) to the experimental data of Rudd *et al.* [12]. The sum of ion yield (corrected due to kinetic energy release) of all different product ions for processes that release at least one electron is now normalized to the value of equation (2) for each proton energy. This calibration procedure generates absolute partial cross-section curves for the various product ions in the energy range from 20 to 150 keV.

Figure 5b shows the presently determined partial ionization cross-sections upon proton impact for events that release at least one electron (filled symbols) in comparison to the data of Werner *et al.* [14] (open symbols). In addition the dashed lines represent fits of equation (2) to the partial cross-sections including both data sets (the present one and that of Werner *et al.*). The present values smoothly extend the high-energy data of Lutz and coworkers to the low energy side. The shape of the partial cross-sections shown in Figure 5b reveals especially at lower energies distinct differences. Whereas the cross-section for the production of the H_2O^+ reveals a very flat shape, the partial cross-sections for the fragment ions show a more and more pronounced maximum when going from OH^+ and H^+ to O^+ and O^{2+}. Furthermore, the maximum in the partial cross-sections is positioned at about 70 keV for H_2O^+, 78 keV for OH^+, 74 keV for H^+, 65 keV for O^+, and 38 keV for O^{2+}. It seems to be rather strange that the maximum for the production of the ion that needs most energy to be formed is at the lowest proton energy. However, it has to be mentioned that at low collision energies O^{2+} can be formed also by electron capture processes (neutralization of the projectile but still with emission of an electron). For all other fragment ions the contribution due to double ionization upon electron capture processes can be neglected. These events will be observed as two singly charged ions in coincidence with a neutralized projectile. This shows that the knowledge of the final charge state of the projectile ion leads to more information about the actual collision process than the previous experiments could provide.

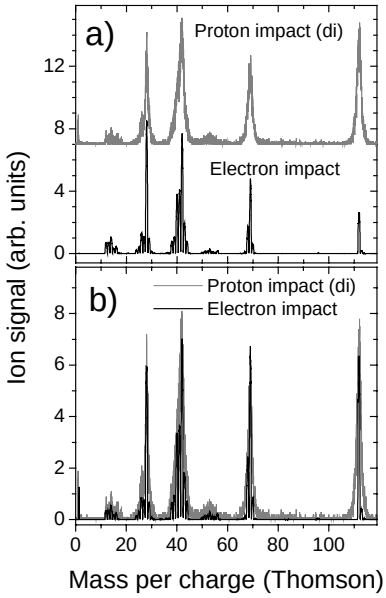

Fig. 6. Mass spectrum of the product ions measured by electron impact ionization in Innsbruck (black line) by 200 eV electrons in comparison to a mass spectrum measured by proton impact ionization (gray line) with the Lyon apparatus in coincidence with an unchanged charge state of the p^+ projectile (direct ionization). The upper part (a) shows the original mass spectra and in the lower part of this figure (b), the Innsbruck data were multiplied with a quadratic function in order to achieve similar peak heights for the whole mass range (see text).

4 Proton and electron impact ionization of uracil molecules

Figure 6 shows first preliminary results for proton impact ionization of uracil that was evaporated at 460 K from an oven (gray line). The charge state of the projectile after the collision was unchanged (direct ionization) and in order to increase the statistics the data from all collision energies ranging from 20 keV to 150 keV were added up. In addition to the proton impact data the dark line shows a mass spectrum measured in Innsbruck using electron impact ionization. Figure 6a shows the original mass spectra

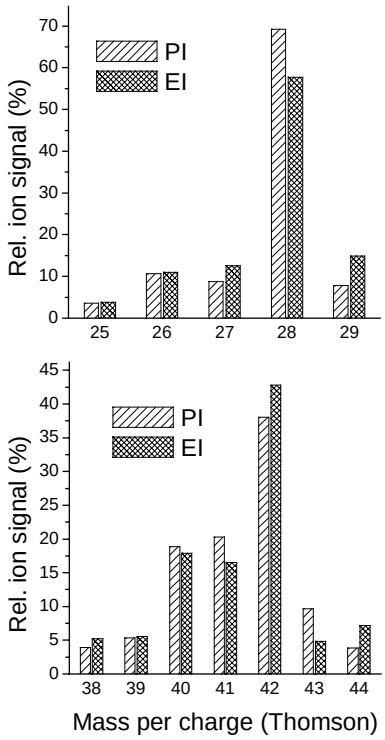

Fig. 7. Relative areas of the Gaussian curves that fit best the peaks of the mass spectrum shown in Figure 3 (single hatched bars). The cross hatched bars are the relative areas of the corresponding mass peaks measured with electron impact ionization shown in Figure 5.

and in Figure 6b the Innsbruck electron data were multiplied with a quadratic function of the electron energy in order to achieve similar peak heights for the two mass spectra. The electron energy was set to 200 eV and the temperature of the uracil oven was set to 461 K. Like in the case of water the detection efficiency for fragment ions might be reduced in both instruments. Furthermore, the quadrupole mass filter used in Innsbruck was optimized for maximum transmission of the H^+ fragment ion which certainly reduced the transmission of heavier ions through the mass spectrometer.

It is interesting to note that both ionization methods lead to the same fragment ions and that the shape of the mass spectra does not differ too much. The mass resolution of the TOF used for the proton impact does not allow the separation of the single mass peaks within the 7 differently sized ion groups containing 1 to 5 of the heavy atoms (C, N or O) or the intact molecule, respectively. Nevertheless the peak pattern obtained by electron impact measured in Innsbruck matches nicely to these unresolved peaks. In Figure 3 we fitted a series of Gaussian curves (with centers at integer mass per charge ratios) to the mass peaks measured by proton impact ionization. Figure 7 shows for two of these ion groups the area of these best fits in comparison to the area of the single peaks measured by electron impact ionization shown in the corresponding mass spectrum in Figure 6. Also for the other ion groups (not shown in Fig. 7) the calculated peak pattern

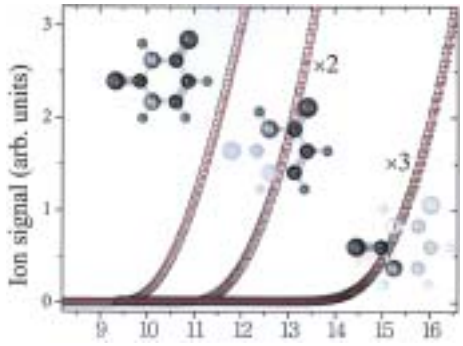

Fig. 8. Ion efficiency curves for the uracil parent ion (mass 112 Dalton) and two fragment ions (mass 69 and 42 Dalton). The structures indicate the bonds that have to break to obtain the corresponding fragment starting from the left structure of Figure 1.

for the Gaussian fits agrees similarly well with the mass peaks measured by electron impact ionization. This suggests that at least for large enough excitation energy uracil decays in a similar fashion into the same fragment ions independent of the ionization mechanism (in the present case proton and electron impact ionization). However, one has to keep in mind that especially the fragment ions may be detected with strongly reduced probability due to the kinetic energy they acquire during the formation process such as Coulomb repulsion of a decaying multiply charged intermediate ion [41].

The measurements in Innsbruck on uracil were performed with an electron monochromator instrument to determine accurately the ionization energies of the various product ions. In the present investigation we determined the appearance energies for the parent ion $C_4H_4N_2O_2^+$ (mass per charge ratio 112 Thomson) and the two most abundant fragment ions $C_3H_3NO^+$ and CNO^+ (mass per charge ratios 69 and 42 Thomson, respectively). Figure 8 shows the threshold region of the ion efficiency curves for these three ions. The lines through the data points indicate fits according to equation (1) allowing us to deduce for the first time accurate appearance energies for these ions. In Table 1 the averaged appearance energies derived from three different measurements for each of these ions are listed in comparison with earlier determinations [42] where available. Electron impact ionization and the method of loosing was utilized in both earlier studies to determine the appearance energies. However, the errors given in reference [39] seem to be unrealistically small since the electron energy resolution was larger than 0.5 eV (typical electron energy distribution from a hot filament without using an electron monochromator). The vertical ionization energy of uracil determined by UV-photoelectron spectroscopy (see Tab. 1 and Ref. [43]) are in good agreement with the presently determined value of the appearance energy of the parent ion.

Except for the missing hydrogen atom at the CNO^+ product ion the two fragment ions $C_3H_3NO^+$ and CNO^+ represent two complementary parts of the uracil molecule and are formed with similar abundance. Nevertheless the

Table 1. Appearance energies for ions produced by electron impact ionization (EI) in comparison to photoelectron (PE) studies of uracil.

Ion	m/z (Thomson)	AE(eV) $\pm\Delta(AE)$	Method	Authors
uracil	112	9.59 ± 0.06	EI	present
$C_3H_3NO^+$	69	10.87 ± 0.04	EI	present
CNO^+	42	13.39 ± 0.02	EI	present
uracil	112	9.82 ± 0.1	EI	Lifshitz *et al.*
uracil	112	9.53 ± 0.02	EI	Zaretskii *et al.*
uracil	112	9.20	PE	Yu *et al.*
uracil	112	9.68	PE	Palmer *et al.*
uracil	112	9.60	PE	Dougherty *et al.*
uracil	112	9.45	PE	Lauer *et al.*
uracil	112	9.50 ± 0.03	PE	Hush *et al.*
uracil	112	9.53	PE	Kubota *et al.*
uracil	112	9.59	PE	Padva *et al.*

ionization energy for the lighter fragment ion CNO^+ is much higher than that for the $C_3H_3NO^+$ ion. The occurrence of the CNO^+ ion (as opposed to the occurrence of the $CNOH^+$ ion), the approximately equal abundance of the two complementary ions and the occurrence of a relatively strong CO^+ ion signal all indicate that in the present study most of the target molecules were present in the tautomeric form presented in the left part of Figure 1. Nevertheless, the occurrence of the COH^+ ion albeit in small abundances (see Fig. 7) indicates also the possible presence of the other tautomeric form in our molecular beam.

In concluding the present work is the first study in a series of collaborative investigations between the two laboratories where ionization and fragmentation of a molecule of biological relevance will be studied parallel with electron and proton impact. Although the mass resolution of the TOF instrument used in Lyon for the proton impact ionization is not sufficiently high to resolve the fragment ions with a mass per charge ratio larger than 20 Thomson a fit through the experimentally determined peaks indicates that the two different projectiles, *i.e.* electrons and protons, lead to the same breakup patterns.

Work partially supported by the FWF, ÖAW and ÖNB, Wien, Austria. We would also like to thank the French and Austrian governments for supporting this research in the frame of the Amadee program and the European Commission, Brussels.

References

1. B. Boudaiffa, P. Cloutier, D. Hunting, M.A. Huels, L. Sanche, Science **287**, 1658 (2000)
2. E.W. McDaniel, J.B.A. Mitchell, M.E. Rudd, *Atomic Collisions* (Wiley, New York, 1993)
3. See Molecules of Biological Interest in the Gas Phase, *Experimental Tools and Quantum Chemistry EuroConference, Euresco Conference*, Centre de Physique, les Houches, France, 13-18 May 2000
4. C.S. Enos, A.R. Lee, A.G. Brenton, Int. J. Mass Spectrom. Ion Proc. **104**, 137 (1991)
5. T.J. Dolan, J. Phys. D **26**, 4 (1993)
6. T.D. Märk, G.H. Dunn, *Electron impact ionization* (Springer, Wien, 1985)
7. V. Tarnovsky, H. Deutsch, K. Becker, J. Chem. Phys. **109**, 932 (1998)
8. L.H. Toburen, M.Y. Nakai, R.A. Langley, Phys. Rev. **171**, 114 (1968)
9. L.H. Toburen, W.E. Wilson, J. Chem. Phys. **66**, 5202 (1977)
10. M.A. Bolorizadeh, M.E. Rudd, Phys. Rev. A **33**, 888 (1986)
11. L.H. Toburen, W.E. Wilson, R.J. Popowich, Radiat. Res. **82**, 27 (1980)
12. M.E. Rudd, T.V. Goffe, R.D. DuBois, L.H. Toburen, Phys. Rev. A **31**, 492 (1983)
13. J.H. Miller, W.E. Wilson, S.T. Manson, M.E. Rudd, J. Chem. Phys. **86**, 157 (1987)
14. U. Werner, K. Beckord, J. Becker, H.O. Lutz, Phys. Rev. Lett. **74**, 1962 (1995)
15. H. Tawara, A. Russek, Rev. Mod. Phys. **45**, 178 (1973)
16. L.H. Toburen, IAEA-TECDOC **799**, 47 (1995)
17. H. Knudsen, U. Mikkelsen, K. Paludan, K. Kirsebom, S.P. Moller, E. Uggerhoj, J. Slevin, M. Charlton, E. Morenzoni, J. Phys. B **28**, 3569 (1995)
18. M. Fieber, Ph.D. thesis, Technische Universität Berlin, 1991
19. B. Farizon, M. Farizon, M.J. Gaillard, R. Genre, S. Louc, J. Martin, J.P. Buchet, M. Carré, G. Senn, P. Scheier, T.D. Märk, Int. J. Mass Spectrom. Ion Proc. **164**, 225 (1997)
20. B. Farizon, M. Farizon, M.J. Gaillard, F. Gobet, M. Carré, J.P. Buchet, P. Scheier, T.D. Märk, Phys. Rev. Lett. **81**, 4108 (1998)
21. G. Hilbert, T.B. Johnson, J. Am. Chem. Soc. **52**, 2001 (1931)
22. G.A. Howard, B. Lythgoe, R. Todd, J. Am. Chem. Soc. 1052 (1947)
23. C. Desfrançois, V. Périquet, Y. Bouteiller, J.P. Schermann, J. Phys. Chem. **102**, 1274 (1998)
24. N.A. Oyler, L. Adamowicz, J. Phys. Chem. **97**, 11122 (1993)

25. R. Pazdur *et al.*, Proc. Am. Soc. Clin. Oncol. **18**, 1009a (1999)
26. C. Desfrançois, H. Abdoul-Carime, J.P. Schermann, J. Chem. Phys. **104**, 7792 (1996)
27. M. Carré, M. Druetta, M.L. Gaillard, H.H. Bukow, M. Horani, A.L. Roche, M. Velghe, Mol. Phys. **40**, 1453 (1980)
28. B. Farizon, M. Farizon, M.J. Gaillard, Int. J. Mass Spectrom. Ion Proc. **192**, 259 (1999)
29. W.C. Wiley, I.H. McLaren, Rev. Sci. Instrum. **16**, 1150 (1955)
30. D.W. Koopman, Phys. Rev. **166**, 57 (1968)
31. M.E. Rudd, Akio Itoh, T.V. Goffe, Phys. Rev. A **32**, 2499 (1985)
32. G. Denifl, D. Muigg, A. Stamatovic, T.D. Märk, Chem. Phys. Lett. **288**, 105 (1998)
33. D. Muigg, G. Denifl, A. Stamatovic, O. Echt, T.D. Märk, Chem. Phys **239**, 409 (1998)
34. T. Fiegele, G. Hanel, I. Torres, M. Lezius, T.D. Märk, J. Phys. B **33**, 4263 (2000)
35. G.H. Wannier, Phys. Rev. **90**, 817 (1953)
36. W.G. Mallard, P.J. Linstrom (2000) NIST Standard Reference Database E Vol. 69 (Gaithersburg: National Institute of Standards and Techznology) webpage `http://webbook.nist.gov`
37. T. Fiegele, N. Mason, V. Foltin, P. Lukac, A. Stamatovic, P. Scheier, T.D. Märk, Int. J. Mass Spectrom. **209**, 23 (2001)
38. T.J. Morgan, K.H. Berkner, W.G. Graham, R.V. Pyle, J.W. Stearns, Phys. Rev. A **14**, 664 (1976)
39. P. Scheier, G. Senn, S. Matt, T.D. Märk, Int. J. Mass Spectrom. Ion Proc. **172**, L1 (1998)
40. F. Gobet, B. Farizon, M. Farizon, M.J. Gaillard, M. Carré, M. Lezius, P. Scheier, T.D. Märk, Phys. Rev. Lett. **86**, 3751 (2001)
41. P. Scheier, B. Dünser, T.D. Märk, Phys. Rev. Lett. **74**, 3368 (1995)
42. C. Lifshitz, E.D. Bergmann, B. Pullman, Tetrahedron Lett. **46**, 4583 (1967); V.I. Zaretskii, V.L. Sadovaskaya, N.S. Wulfson, V.F. Sizoy, V.G. Merimson, Org. Mass Spectrom. **5**, 1179 (1971)
43. C. Yu, T.J. O'Donnell, P.R. LeBreton, J. Chem. Phys. **85**, 3851 (1981); A. Padva, P.R. LeBreton, R.J. Dinerstein, J.N.A. Ridyard, Biochem. Biophys. Res. Commun. **60**, 1262 (1974); M. Kubota, T. Kobayashi, J. Electron Spectros. **82**, 61 (1996); D. Dougherty, K. Wittel, J. Meeks, S.P. McGlynn, J. Am. Chem. Soc. **98**, 3815 (1976); N.S. Hush, A.S. Cheung, Chem. Phys. Lett. **34**, 11 (1975); G. Lauer, W. Schäfer, A. Schweig, Tetrahedron Lett. **45**, 3939 (1975); M.H. Palmer, I. Simpson, R.J. Platenkamp, J. Mol. Struct. **66**, 243 (1980)